Acta Materialia 215 (2021) 117078

Contents lists available at ScienceDirect

Acta Materialia

journal homepage: www.elsevier.com/locate/actamat

Full length article

Theory of kink migration in dilute BCC alloys

Alireza Ghafarollahi [a,*], W.A. Curtin [a]

Laboratory for Multiscale Mechanics Modeling (LAMMM), Institute of Mechanical Engineering, EPFL, 1015 Lausanne, Switzerland

ARTICLE INFO

Article history:
Received 23 March 2021
Revised 7 June 2021
Accepted 7 June 2021
Available online 16 June 2021

Keywords:
BCC
Dilute alloys
Kink migration
Screw dislocations
Solute strengthening

ABSTRACT

Plastic deformation in elemental BCC metals and dilute alloys is controlled by the slower of the kink pair nucleation and kink migration processes along screw dislocations. In alloys nucleation is facilitated and migration inhibited, leading to a concentration- and temperature-dependent transition from nucleation dominance to migration dominance. Here, an analytical statistical model for the stress-dependent kink migration barrier in dilute BCC alloys is developed and validated. The barrier depends only on a clearly-defined solute/screw dislocation interaction parameter, the kink width, and dislocation length between jogs. The analytic model is extensively validated via fully atomistic nudged-elastic band calculations and stochastic simulations in a model Fe-Si alloy. Combined with a recent validated double-kink nucleation theory, a fully-analytic model for the temperature- and concentration-dependent flow stress is obtained that includes the transition from nucleation to migration control. The overall model is applied to Fe-Si and W-Re using independently-determined material properties and good agreement is obtained with experiments over a range of concentrations and temperatures. Overall, the two theories represent a unified, fully-statistical, parameter-free understanding of screw dislocation strength in dilute BCC alloys.

1. Introduction

The temperature-dependent plasticity of BCC metals and dilute substitutional alloys is controlled by the motion of $1/2\langle 111\rangle\{110\}$ screw dislocations between local energy minima (Peierls valleys at spacing a) by a two-step thermally-activated process [1–4]. The first step is nucleation of a pair of kinks somewhere along an initial long straight screw dislocation. The second step is the migration of these kinks along the screw dislocation of length L, where $L = 1/\sqrt{\rho}$ is estimated as the distance between dislocation junctions/jogs at dislocation density ρ. These steps lead to a plastic displacement of a for each dislocation segment. The macroscopic plastic strain rate due to the motion of all N dislocations is then consistent with Orowan's law $\dot{\epsilon} = Nab/L^2\bar{t} = \rho ba/\bar{t}$ where $\bar{t}$ is the average time for the two-step process [2,4–6]. Nucleation and migration processes each have stress-dependent activation energies $\Delta H(\tau)$ and the rate-controlling process is the one with the higher activation energy and longer time $\bar{t} \sim \exp(\Delta H(\tau)/kT)$.

In pure BCC metals, flow is controlled by the double-kink nucleation process because kink migration has a negligible barrier. In dilute random alloys, the added solutes affect the activation energies for both nucleation and migration processes [7,8]. Generally, solutes reduce the nucleation barrier, as understood theoretically [1,2,9] and observed experimentally [1,10], because nucleation always occurs in a region along the dislocation line where the local solute fluctuations in the random alloy most-favor double-kink formation. In contrast, solutes increase the kink migration barrier because the kinks must overcome the largest barrier(s) created by the extreme solute statistical fluctuations along the remaining line. Since stress provides a driving force for overcoming barriers and since longer lengths will have larger extreme fluctuations somewhere along the length, it becomes critical to accurately determine the stress- and length-dependent barriers $\Delta H_{\rm dk}(\tau, L)$ and $\Delta H_{\rm km}(\tau, L)$ for nucleation and migration, respectively, in a random alloy.

Note that any model that embodies the above two effects of the solutes in some manner will predict a transition from nucleation to migration control of strength. Predicting a transition is thus not sufficient validation of a model. Furthermore, models that involve adjustable parameters allow for the transition to be tuned to match data, and so again are not sufficient validation. Historical models for nucleation and migration do not fully handle the energetic and statistical aspects of the problem [2,5,6]. These models simplify the solute/screw dislocation interactions to a single value E and then use approximate statistics to estimate

* Corresponding author.
E-mail address: alireza.ghafarollahi@epfl.ch (A. Ghafarollahi).

https://doi.org/10.1016/j.actamat.2021.117078

the effects of solute fluctuations. The Suzuki model predicts a reduced barrier for nucleation but the model of Trinkle and Woodward does not (see [11] for more discussion). For kink migration, Suzuki [2] considered the statistical number of accumulated solute atoms $m(z)$ around the screw core that have been passed during the movement of the kink a distance z along the dislocation line with barrier $\Delta H_{km} = m(z)E - \tau zab$ where b is the Burgers vector and $a = 0.943\,b$. The kink width w was then introduced by averaging the barrier over $z \pm w/2$. Trinkle and Woodward [5,6] approximated the barrier as $\Delta H_{km} = m|E|$ with fixed $m = 25\sqrt{c}$, or other related forms, as an estimate of the largest cluster, with no accounting for kink width. Kinetic Monte Carlo methods have also been used recently to model both double-kink and kink-migration in dilute alloys [12–14]. The formulations ensure that a transition is obtained but treatment of the kink structure, solute/screw interactions, and/or solute effects on the nucleation barrier remain approximate.

We note that after the transition from double-kink nucleation to kink migration control has occurred, additional phenomena are possible. In particular, when the kink migration barriers are high (low stress, high temperature), it is possible that more than one double-kink can nucleate along the same dislocation segment. If this nucleation occurs on one of the other crystallographically-equivalent slip systems, the eventual intersection of two kinks on different planes gives rise to cross-kinks. Cross-kinks form strong pinning points that are only broken by formation of vacancy or self-interstitial point defects, and so contribute to strengthening. This phenomenon tends to arise in the non-dilute regime, and is incorporated into various theories [2,15] and can occur in KMC simulations [16–19]. This topic is beyond the scope of the present paper.

Here, we develop a rigorous statistical model for the effect of solutes on the kink migration barrier as a function of concentration and applied stress. Interactions of all solutes at all distances from the straight and kinked screw are considered, as in our previous model of double-kink nucleation. The model for the kink migration barriers is validated against direct atomistic nudged elastic band (NEB) calculations and related stochastic simulations on a model Fe-Si alloy. We then show that the kink migration process under stress is essentially the random walk-type "Wiener process with drift", which yields analytic results for the barrier in terms of all relevant material properties. The resulting model for the kink migration barrier as a function of stress, solute concentration, and dislocation length is fully compatible with our previous analytic solution for the double-kink nucleation barriers, enabling natural predictions of the transition from nucleation to kink control of strength as function of temperature and strain rate in any dilute alloy. Application to real dilute Fe-Si with independent inputs show that kink migration becomes controlling around 3% Si. Application to real dilute W-Re up to 7%Re using DFT calculations of the W-Re screw interaction energies and other independent inputs also show good agreement for the transition from nucleation softening to migration strengthening at T=300K and above.

The remainder of the paper is organized as follows. In section 2, we discuss the effect of multiple solutes on the kink migration barrier. The statistical models to predict the double-kink nucleation barrier as a function of solute concentration and dislocation length are presented. In Section 3, we validate our analytic statistical model using atomistic simulations on a model Fe-Si alloy. Section 4 is devoted to the effect of applied stress on the kink migration. The Wiener process is adapted to the kink-migration problem in this section. In Section 5, we discuss the general application of our results and make specific comparisons for Fe-Si and W-Re real alloys. 6 discusses our results further and summarizes them.

2. Solute effects on the kink migration barrier

2.1. Solute/kink interaction energy

We consider a dilute binary alloy with "solute" atoms at concentration $c << 1$ and "matrix" atoms at concentration $1 - c$. The model is easily generalized to multiple components and non-dilute concentrations. For a dislocation at the origin $x = y = 0$ lying along the z direction, a solute at lattice site (x_i, y_j) has an interaction energy $U(x_i, y_j)$ with the dislocation, independent of the z coordinate due to translational invariance. When the dislocation glides by a along the glide direction x, the energy of the same solute has an interaction energy $U(x_i - a, y_j)$, and the change in interaction energy is then denoted as $\Delta U_{ij}(a) = U(x_i - a, y_j) - U(x_i, y_j)$.

After double-link nucleation, the two kinks propagate away from each other through the random field of solutes. The two kinks are assumed to be independent, neglecting their very small elastic interactions. We thus focus on a single kink. The kink is the structure that shifts the screw dislocation from the initial to the final Peierls valley. The shape of the kinked dislocation with the kink centered at z_c and gliding in the positive z-direction is commonly described by a hyperbolic tangent function [20,21]. We thus describe the kinked dislocation as

$$x(z - z_c; w) = \frac{a}{2}\left(1 - \tanh\left[\frac{2(z - z_c)/b}{w/b}\right]\right) \tag{1}$$

where w denotes the kink width defined as distance between the intersections with the adjacent Peierls valleys of a tangent line at the kink inflection (see Fig. 1a). Estimates and models show that $w \sim 10 - 20b$ is typical, so that the kink character is very nearly screw (character angle at most $\tan^{-1}(2a/w) \approx 5^\circ$).

We must compute the total energy change $\Delta E(z_c)$ of the system (dislocation plus solutes) as a function of the center position z_c of the kink as it glides across the segment length ($0 < z_c < L$). Here, we assume a model for the solute/kink interaction energies and validate that assumption via direct simulations in Section 3.2. The solute/dislocation interaction energy should vary smoothly from $U(x_i, y_j)$ to $U(x_i - a, y_j)$ as the kink glides past the solute, and this total change is independent of the kink shape. Thus, although the theory is developed by carefully considering the solute/kink interactions, the final results emerge to be weakly dependent on the actual kink width and shape (see Eq. (10)). Since the kink shape is very nearly screw-like at either end, i.e. at $|z - z_c| \to \pm w/2$, the solute interaction energies in these regions are very nearly those of the straight screw. Here, we assume that the interaction energy between a solute at (x_i, y_j, z_k) and a kinked dislocation with kink centered at z_c is proportional to the normalized square of the kink position relative to the nearest Peierls valley in the same z_k plane as the solute. This effective kink shape is shown schematically in Fig. 1(a); it is essentially identical to the original kink shape but with an effective kink width $w^* = 0.5w_k$. Therefore, the solute/kinked-dislocation interaction energy is approximated as

$$U\left(x_i, y_j, z_k, z_c; w^*\right) = \frac{x(z_k - z_c; w^*)}{a}\Delta U_{ij}(a) + U_{ij}. \tag{2}$$

In this approximation, the kink is assumed rigid, i.e. not affected by the solutes, which is also implicit in prior screw strengthening theories [2,5]. Nevertheless, using the NEB method as described later, we have examined variations in the kink shape as it glides through a random atomistic in Fe-4 at.%Si model alloy that has significant solute/dislocation interactions. Among hundreds of specific random solute environments, we find very little, if any, change in kink shape and width.

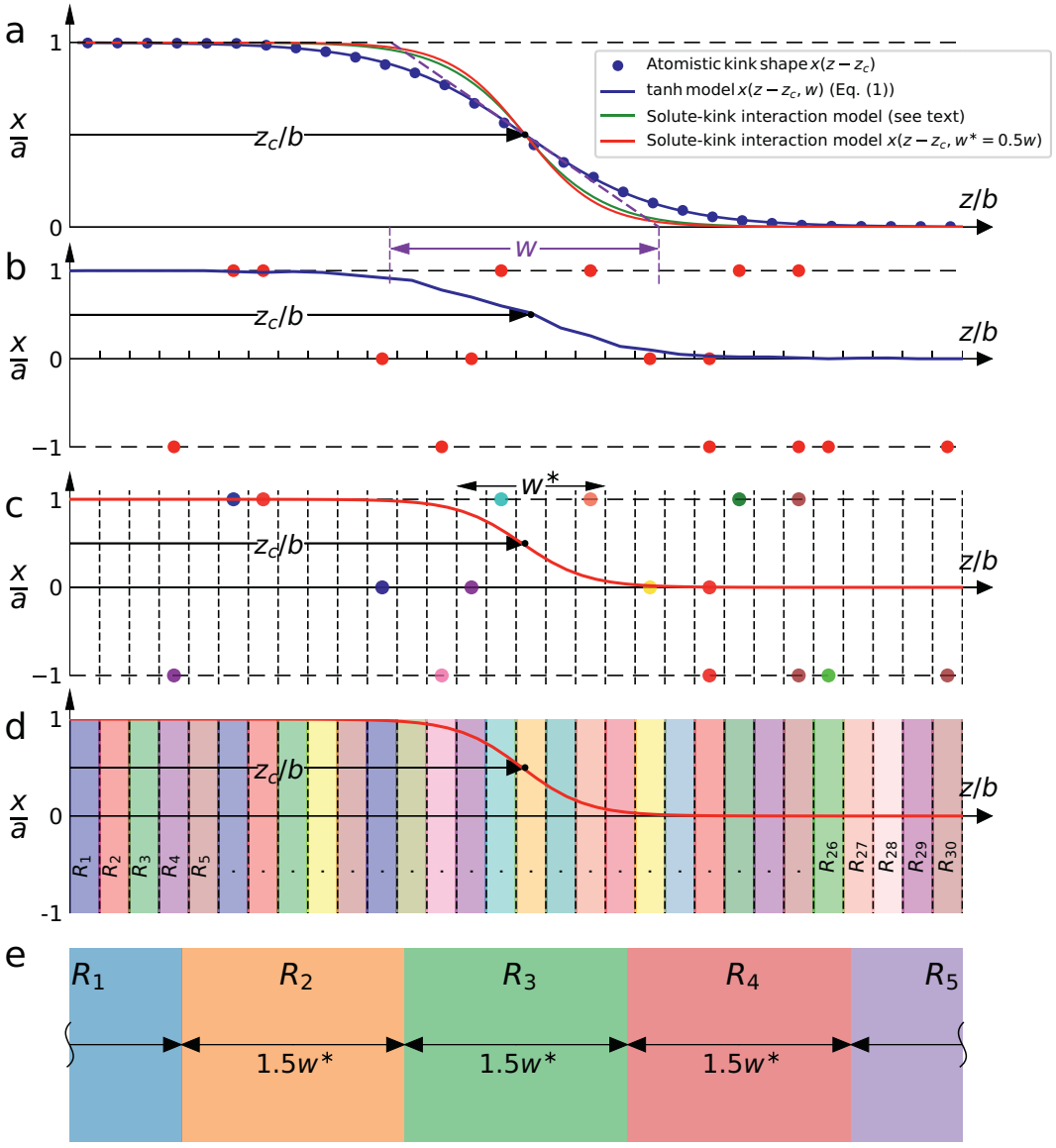

Fig. 1. (a) Schematic of the models for the kink shape and solute/kink interaction energy. The atomistic kink shape in the pure metal is described by a hyperbolic tangent function Eq. (1) with kink width w defined by the geometric constuction shown. The solute/kink interaction energy (Eq. (2)) is related to the square of the distance of the kink to the nearest Peierls valley, which is nearly identical to a tanh function with effective kink width $w^* = w/2$ as shown. **(b,c,d,e) Schematic of models developed here for determining the energy landscape of single kink migration across a random field of solutes.** (b) Fully-atomistic NEB simulation with a possibly-varying kink shape and all solutes interacting with all portions of the dislocation line; (c) Discrete Rigid-Kink Model (DRKM) with solute/kink interactions governed by the effective kink shape (effective width $w^* = 0.5w$) and interactions of each solute at z_k scale with the relative distance $z_k - z_c$; (d) Stochastic Rigid-Kink Model (SRKM) where the total solute/dislocation interactions at z_k are replaced by a single stochastic value $R_i \Delta\tilde{E}_p$ chosen from the statistical distribution of the solute/dislocation interaction energies where R_i is a random number chosen from a Gaussian probability distribution of mean zero and unit standard deviation; (e) Wiener Process Model (WPM) where the dislocation is divided into $L/1.5w^*$ statistically uncorrelated segments each of which is assigned an energy $R_i \Delta E_p (1.5w^*/b)^{1/2}$ where R_i is a random number chosen from a Gaussian probability distribution of mean zero and unit standard deviation randomly selected from a normal distribution with zero mean and standard deviation. This model does not involve the kink shape, only the decorrelation length $1.5w^*$ of the solute/kink interaction.

2.2. Energy landscape models for kink glide

Here, we present a sequence of models for determining the energy landscape experienced by a kink gliding through a random field of solutes. A schematic illustration of these models is shown in Fig. 1.

Using Eq. (2) for the single solute/kink interaction energy, the total interaction energy of the solutes with a kink centered at z_c is simply the sum of the interaction energies contributed by each individual solute in the specific configuration of solutes in the random alloy,

$$U(z_c) = \sum_{i,j,k} s_{ijk} U(x_i, y_j, z_k, z_c; w^*) \tag{3}$$

where the site occupation variable $s_{ijk} = 1$ if a solute is at position (x_i, y_j, z_k) and 0 otherwise. The energy landscape that determines the overall kink migration corresponds to the total solute/dislocation energy change as a function of the migration distance starting from an initial position $z_c = z_0$ to the current z_c, which can now be written as

$$\Delta E(z_c) = \sum_{i,j,k} s_{ijk} \frac{x(z_k - z_c; w^*) - x(z_k - z_0; w^*)}{a} \Delta U_{ij}(a) \tag{4}$$

We call this model for the energy landscape of the migrating kink the Discrete Rigid-Kink Model (DRKM); a schematic is shown in Fig. 1c. The DRKM differs from the true atomistic problem only by the assumed solute/kink interaction model and rigid kink shape.

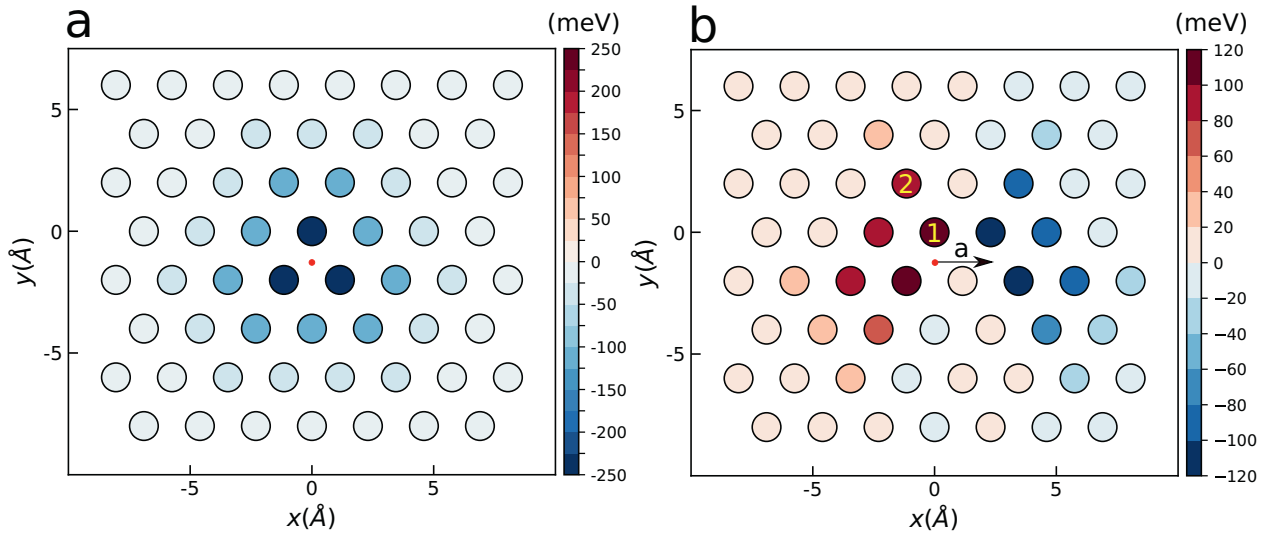

Fig. 2. (a) Solute/screw interaction energy U_{ij} versus solute position for single Si solute in Fe matrix computed using the EAM potential of [14]. (b) Interaction energy difference $\Delta U_{ij}(a)$, as the screw dislocation core moves by one Peierls valley distance a (black arrow). Sites marked with 1 and 2 are substituted with Si atoms for subsequent NEB calculations, and are referred to in Fig. 3.

The DRKM energy landscape is for one specific configuration of random solutes. A further simplification is required to ultimately achieve an analytic model. We first note that the statistical average of the solute/kinked dislocation interaction energy change is zero, $\langle \Delta E(z) \rangle = 0$, where the average is taken over the stochastic variable s_{ijk}. Thus, only the statistical fluctuations lead to energy variations with position, as discussed in [11]. The relevant statistical quantity is the standard deviation in the interaction energy change per Burgers vector of line length. For a straight segment of dislocation, the standard deviation can be computed as [11,22]

$$\Delta\tilde{E}_p = \left(\sum_{ij} c\, \Delta U_{ij}(a)^2 \right)^{\frac{1}{2}} \tag{5}$$

Then, within our solute/kinked-dislocation interaction energy model, each individual section of material of width b perpendicular to the dislocation line has some random set of solute positions that dictate the contribution to the total energy at that position z. The fluctuations in this energy over all possible solute configurations are proportional to $\Delta\tilde{E}_p$ and to the dislocation position $x(z - z_c; w)$. The energy of each section of width b with the kink at position z_c is thus $R\Delta\tilde{E}_p x(z - z_c; w^*)/a$ where R is a random number selected from a Gaussian probability distribution having zero mean and standard deviation of unity. For a dislocation segment of length $L = N\,b$ the energy landscape can then be written as

$$\Delta E(z_c) = \Delta\tilde{E}_p \sum_{k=1}^{N=L/b} x(z_k - z_c; w^*)\, R_k \tag{6}$$

We call this model the Stochastic Rigid Kink Model (SRKM), schematically shown in Fig. 1d. This model involves no direct discrete solutes, only the relevant stochastic energy quantity $\Delta\tilde{E}_p$, the kink shape, and a set of random numbers along the line that capture the exact statistical fluctuations due to random solutes, within our approximation for the solute/kinked-dislocation interaction energy.

The above models are representations of the entire energy landscape over a length L in a specific random alloy as a function of the solute/dislocation interaction energies, the kink shape, and the length L. An applied stress is added subsequently as discussed below. From these models, we extract the largest global barrier for kink glide, i.e. the difference between the highest energy and the lowest energy along the entire path in the direction of the kink glide. It is this (stress-dependent) barrier that will control the kink migration over length L.

3. Validation using an atomistic model Fe-Si alloy

We now compare predictions of our analytical model for the solute/kink interaction energy and the stress assisted kink migration enthalpy barrier against direct atomistic simulations using a model Fe-Si alloy. The only input parameters to the model are the solute/screw-dislocation interaction energies $U(x_i, y_j)$ at all distinct solute positions ij around the screw core, the length L of the dislocation, and the single kink shape in the pure matrix material.

3.1. Simulation Details

We use a model Fe-Si alloy system as represented by an EAM potential [14]. The Fe-Fe interactions [23] have all the underlying DFT-based features for Fe screw dislocations such as the compact core structure, the single-hump Peierls potential, and {110} slip-plane. Since we are interested in dilute alloys, we further set Si-Si interactions to those of Si-Fe, eliminating direct solute-solute interactions. Therefore, although not being an accurate representation of real Fe or real Fe-Si, this potential is a well-defined model system that can be used with confidence to validate our analytical model; it was also used previously to study solute effects on double-kink nucleation [22]. The kink shape in pure Fe is determined using the disregistry method [24] and fit to the functional form given by Eq. (1) leading to $w = 10\,b$. The critical solute/dislocation energy change ΔU_{ij} as a function of solute position for this potential is shown in Fig. 2. The key statistical quantity entering the analytic theories is then calculated as $\Delta\tilde{E}_p = 344\,\text{meV}\sqrt{c}$ at Si solute concentration c. We study both $c = 0.01$ and $c = 0.04$, for which $\Delta\tilde{E}_p = 34.4\,\text{meV}$ and $\Delta\tilde{E}_p = 68.8\,\text{meV}$. All quantities entering the model are well-defined and computed independently of the model.

The minimum energy path during kink migration from an initial position to a final position is computed using the nudged elastic band (NEB) method as implemented in LAMMPS. Since kinks

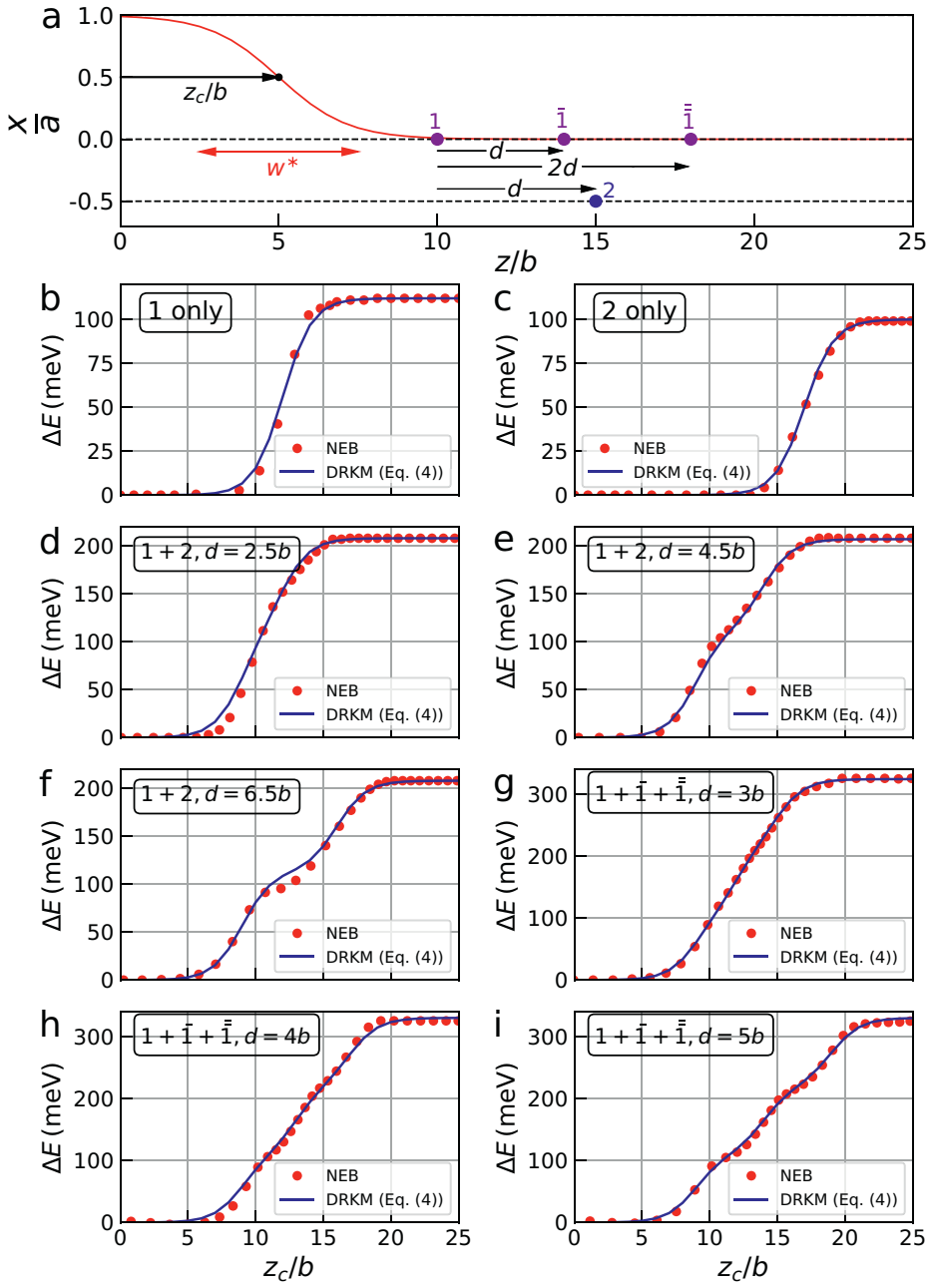

Fig. 3. (a)Schematic of solute positions that are bypassed by a single kink, with similar colors and numbers for solutes in the same atomic row position (x_i, y_j) and corresponding to sites marked in Fig. 2b with $\Delta U_1 = 112$ meV and $\Delta U_2 = 95$ meV. (b)-(i) NEB and predicted kink migration energy versus kink position z_c/b for each special solute arrangement as indicated; e.g. $1+2, d=6.5b$ in (f) denotes solutes at sites #1 and #2 at fixed distance $d = 6.5b$.

must come in pairs, the simulation of motion of a single kink requires special details. We start with pure Fe and create a cell having total dislocation line length longer than the simulated kink glide length $L = 120b$ subsequently studied in the alloy. A single solute is placed in the most energetically favorable location for aiding double-kink nucleation and a second solute placed at $\sim w$ away to inhibit glide of one of the two nucleated kinks. An NEB simulation is then performed during which the double-kink nucleates at the favorable solute and only one kink glides across the remaining length of the simulation cell. A large number of replicas are used so that increments of kink motion between each replica are nearly one b distance. These replicas are then used as the initial path for NEB through a random solute field. More details of the NEB simulation can be found in Appendix A.

3.2. Validation of solute/kink interaction energies

Here we validate the solute/kink interaction model shown in Fig. 1a where the interaction involves the effective kink width $w^* = w/2$. This is achieved by comparing predicted and NEB-computed changes in energy as the kink moves past specific selected arrangements of solutes.

The specific Si solute configurations studied here are shown schematically in Fig. 3(a). For each specific set of solute positions, we calculated the energy landscape of the system as function of kink position z_c using Eq. (4). Direct NEB calculations of the total system energy change are then performed on the exact same solute configurations. Figs. 3(b-i) show the atomistic NEB and predicted energy landscapes of the selected solute configurations. The

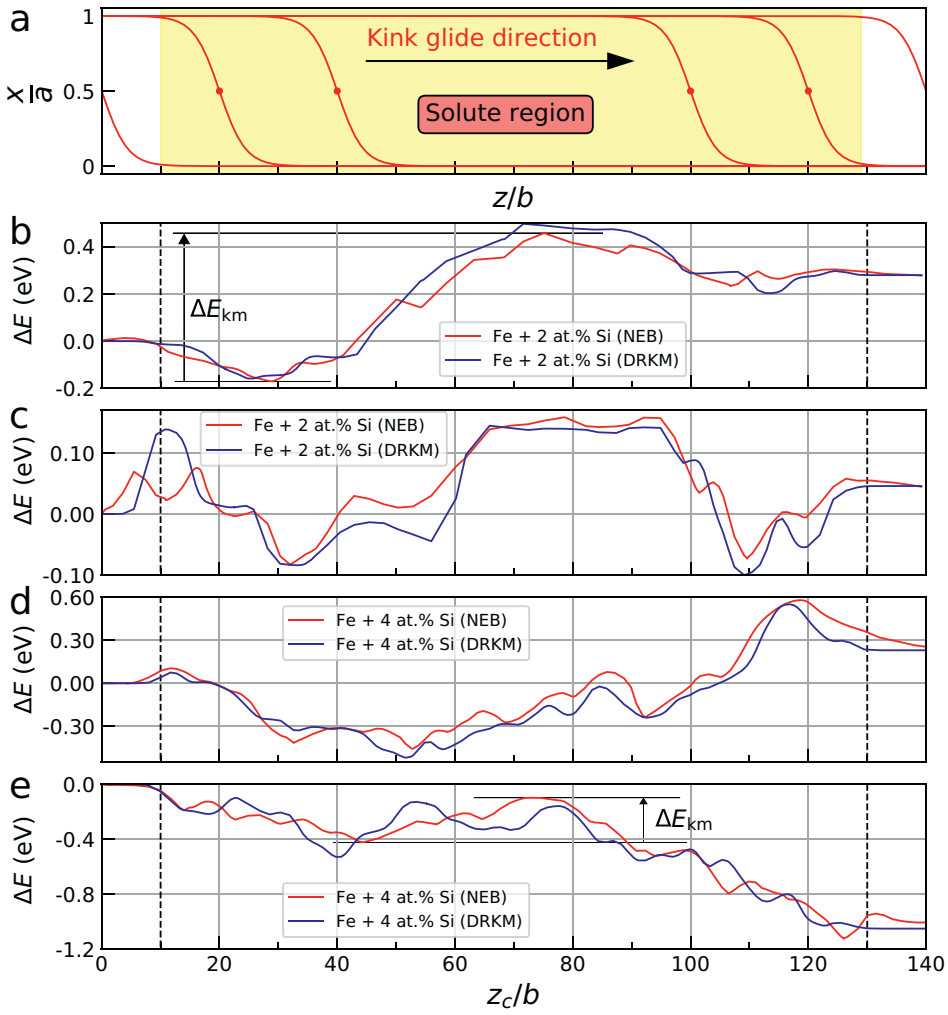

Fig. 4. (a) Schematic of a single kink migrating from left to right through a field of solutes randomly distributed within the yellow-shaded region of length $L = 120b$. (b,c,d,e) Energy landscape as a function of the center position z_c of the kink as computed from direct atomistic NEB and from the Discrete Rigid Kink Model on exactly the same solute configuration, for two typical samples of Fe-1%Si and two typical samples of Fe-4%Si alloys. The largest barrier encountered by the kink for two of the NEB landscapes is indicated as ΔE_{km} for illustration.

agreement is very good in all cases, with deviations of less then ~ 10 meV across all cases. Subsequent similar studies discussed below in fully-random Fe-Si will further confirm, at a statistical level, the agreement between the model and NEB.

3.3. Validation of Kink Migration Models

Here, we validate the Discrete Rigid-Kink Model and Stochastic Rigid-Kink models by comparison against direct fully-atomistic NEB simulations of a single kink migrating across a random field of solutes at zero stress.

In order to perform the NEB simulations of kink migration in random solute field, using the NEB simulation setup generated as discussed in 3.1, a random solute field of the Fe-Si alloy is created by randomly distributing Si atoms at concentration c over a central section of length $L = 120b$ in the simulation cell away from the original double-kink nucleation site. This length is approximately $24w^*$, which is sufficient for validating our models. NEB is then executed to obtain the energy change $\Delta E(z_c)$ as a function of the kink position z_c. We create 200 different realizations of random Si at concentrations 1% and 4% to assess the average barrier and variations around the average with good accuracy. For each individual random distribution of solutes, we have a precise corresponding DRKM simulation.

Example energy landscapes as computed from the NEB and from the DRKM on exactly the same solute configuration are shown in Figs. 4b-e. By definition, the zero of energy corresponds to the energy at the initial kink position when it is first fully within the solute region. The net energy change over the length L can be positive or negative, depending on the overall fluctuations of the particular solute configuration. The DRKM captures the overall full NEB landscape very well in magnitude and length scales of major energy variations. Recall that the DRKM has no adjustable parameters. As expected, the NEB landscape shows additional energy variations on scales smaller than $w^* = 5b$ because the atomistic kink may adapt subtly to the precise solute configurations and because the model for the solute/kink interactions is not exact. Nonetheless, the differences between the NEB and the DRKM are typically below 0.05 eV and 0.1 eV for $c = 1\%$ and $c = 4\%$, respectively, which are small compared to the overall variations of 0.4 eV and 1.0 eV.

The most important quantity controlling the rate of the kink motion is the largest typical energy barrier encountered by the kink over a glide distance z. We have thus extracted the maximum barrier over the length $L = 120b$ from our NEB, DRKM, and SRKM simulations. Fig. 5 shows the average barrier energy and the distribution of barriers over 200 simulations for the NEB and DRKM

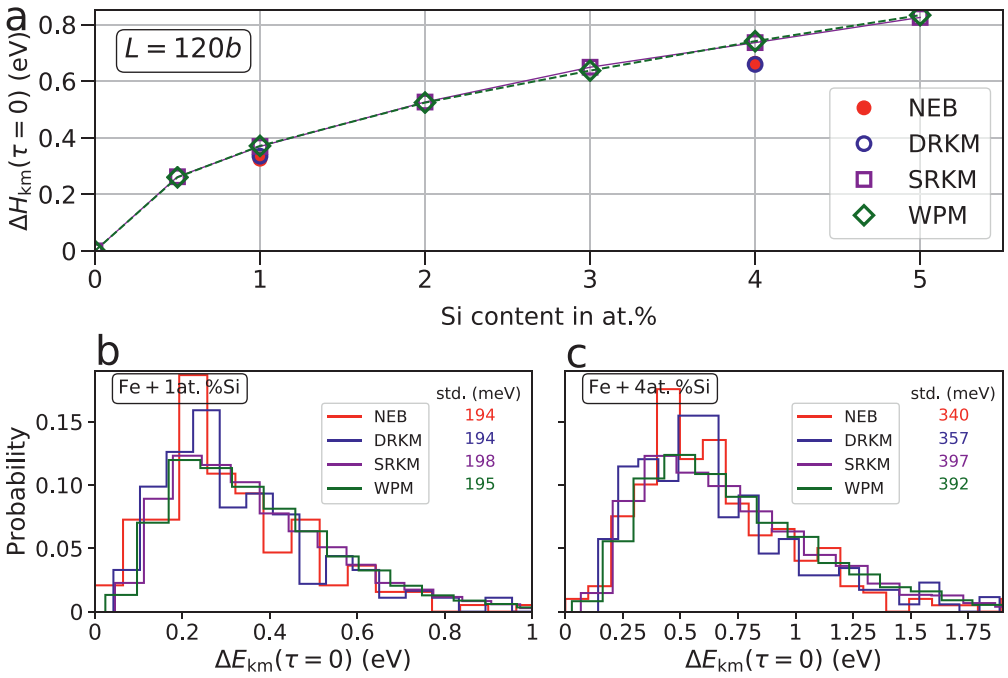

Fig. 5. (a) Average kink migration barrier $\Delta H_{\rm km}$ versus Si solute concentration at zero stress as obtained from NEB, the Discrete Random Kink Model (DRKM), the Stochastic Random Kink Model (SRKM), and the Wiener Process Model (WPM). The distributions of kink migration barriers $\Delta E_{\rm km}$ associated with each models for 200 Fe-1at.%Si and 200 Fe-4at.%Si realizations are also shown, with the standard deviations indicated.

and over ten thousand simulations for the SRKM at c=1% and 4%, and also the average values from the SRKM over a wider range of Si concentrations c. Results are also shown for the Wiener process model (WPM) discussed later. The DRKM captures the average barrier very accurately. The average maximum barrier for the SRKM is slightly higher at both concentrations. The statistical distributions of barriers around the mean all have the same overall shape and magnitude, and the standard deviations are nearly identical. The mean of the SRKM deviates from the NEB and DRKM by less than $\Delta\tilde{E}_p$, which is itself a factor of ~ 6 smaller than the standard deviations of all models. These results quantitatively validate the DRKM and SRKM.

The good agreement between the NEB and the SRKM demonstrates that the dominant energy barriers are controlled by the well-defined solute/dislocation interaction energy parameter. Details of specific solute distributions and deviations of the kink shape from an idealized model are not important in determining the operative distribution of barriers. This is not surprising because the kink is primarily affecting the transition of solute positions relative to the (shifting) dislocation line, and the energy difference at any z once the kink has fully passed by z is captured exactly in the model. This agreement has two important consequences: (i) it justifies the application of the computationally-inexpensive SRKM to examine barriers over length scales L that are much larger than can be studied using direct atomistic NEB or the DRKM and (ii) it points toward the development of an analytic stochastic model.

4. Kink migration under stress

The analyses in the previous section were performed at zero stress. The competition between nucleation and migration is intrinsically stress-dependent, with the applied stress doing work on the system as the double-kinks nucleate and then as the kinks migrate. Here we extend the models and analysis to incorporate the driving force due to an applied shear stress. Specifically, an applied shear stress τ on the glide plane does work (starting from $z_c = 0$) of $-\tau\, b\, a\, z_c$ and hence the energy landscape becomes $\Delta E(z_c, \tau) = \Delta E(z_c, \tau = 0) - \tau\, b\, a\, z_c$. This model assumes a rigid kink, but fluctuations in the area swept due to atomistic changes in kink shape at a fixed mean kink position z_c are negligible.

In the landscape $\Delta E(z_c, \tau)$ with increasing applied stress, the maximum energy barrier $\Delta E_{\rm km}$ and the activation distance z^* between the points of minimum and maximum energies that determine the barrier are both reduced. For each individual energy landscape $\Delta E(z_c, \tau = 0)$ computed from the NEB, DRKM, and SRKM, the stress-dependent kink migration barrier $\Delta E_{\rm km}(\tau)$ is computed as a function of τ. Fig. 6(a) shows the average $\Delta H_{\rm km}(\tau)$ over 200 independent simulations for the NEB and DRKM and over twenty thousand simulations for the SRKM at length $L = 120b$ for c =1% and c =4%. Fig. 6(b) shows the activation distance z^* versus stress, varying smoothly from $\sim L/2$ at $\tau = 0$ to 0 at the stress where $\Delta H_{km} = 0$. The overall agreement is very good. The slightly higher barrier for the SRKM at $\tau = 0$ seen previously is again evident, but the absolute difference then decreases with increasing stress.

4.1. Kink migration under stress: a Wiener Process

The fluctuating energy landscape of a single kink migrating through a random field of solutes over a distance z has several key features: (i) the mean energy change over all possible fluctuations in the solute positions is zero, (ii) the standard deviation of the energy changes due to the fluctuations in the spatial arrangement of solutes scales with $\sqrt{z}$, and (iii) the incremental energy change during kink migration over a distance $z_{c2} - z_{c1} \approx 1.5w^*$ is a stochastic variable. The decorrelation distance of $1.5w^*$ is obtained by examining the correlation function between two kinks separated by $z_{c2} - z_{c1}$, which decreases rapidly from ~ 0.21 at w^* toward zero (~ 0.02) at $1.5w^*$. These features also appear in the random-walk "Wiener process" [25] and so the known solution of the Wiener process can be adapted to address kink migration.

The Wiener process is a continuous-time random walk in which the increments (in our case the energy changes as the kink migrates) are independent. Here, the kink energies become es-

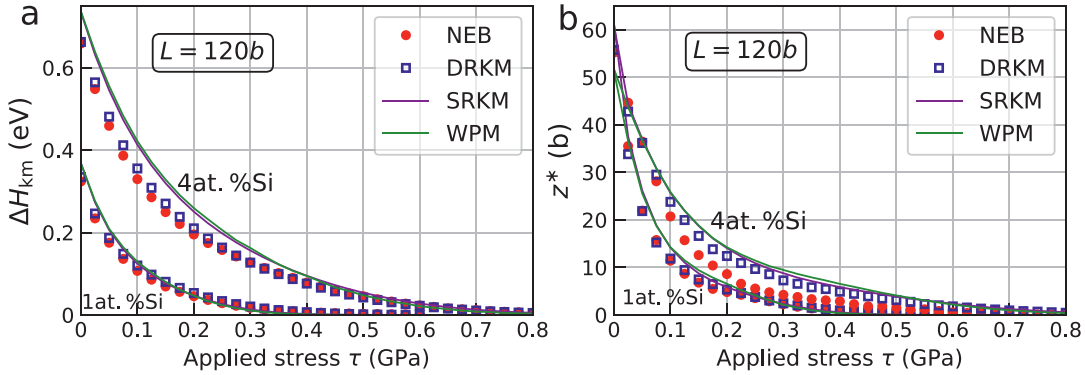

Fig. 6. (a) Average kink-migration barrier $\Delta H_{\rm km}$ and (b) average activation distance z^* versus applied stress τ in model Fe-1at%Si and Fe-4at%Si alloys as obtained from NEB, the Discrete Random Kink Model, the Stochastic Random Kink Model, and the Wiener Process Model.

sentially independent after motion by the decorrelation distance $1.5w^*$. In the presence of an applied stress, the kink migration is then similar to the "Wiener process with drift" where there is a constant-magnitude bias introduced in each step of the random walk. The Wiener process does not appear to capture all the statistical fluctuations of the real energy landscape on the scale of b but it is verified below to capture the all-important mean energy barrier as a function of τ and L. From here on, we will use a normalized kink width $\bar{w} = 1.5w^*/b$ to reduce the notation.

To validate the Wiener process as applied to the kink migration problem, we first execute stochastic simulations at the increment scale of $\bar{w}$ as follows and as shown schematically in Fig. 1e. A dislocation of length L is first divided into $N = L/(b\bar{w})$ sections, each of which is assigned an energy $\Delta\tilde{E}_p\bar{w}^{1/2} \times R_i$ where R_i is a random number selected from a normal distribution with mean zero and standard deviation of unity. A bias energy of $(-ab^2\bar{w})\tau k$ is then added to the k-th segment centered on $z_c/b = k\bar{w}$. The discrete kink-migration energy landscape sampled at discrete $b\bar{w}$ intervals can then be written as

$$\Delta E(k\bar{w}) = \Delta\tilde{E}_p\bar{w}^{1/2}\sum_{i=1}^{k} R_i - (ab^2\tau\bar{w})k, \quad k = 1, 2, \ldots, L/(b\bar{w}) \quad (7)$$

This model is called the Wiener Process Model (WPM).

At zero stress ($\tau = 0$), we compare the mean and standard deviations of the barrier distributions predicted by the WPM against the SRKM for $L = 120b$ ($N = 16$), as shown in Fig. 5. The agreement is essentially perfect. The mean energy barrier versus applied stress as predicted by the WPM is shown in Fig. 6, and again excellent agreement with the SRKM is obtained. To further validate the WPM, we considered longer migration lengths $L/b = 200, 400, 800$ and a range of relevant concentration and stress levels. The comparison between the WPM and the SRKM is shown in Fig. 7, and again the agreement is excellent. *Hence, the physical problem of kink migration in a random solute environment and under stress is quantitatively captured by the random walk Wiener process with drift.*

We now make the final step to an analytic model, eliminating entirely the need for any stochastic simulations. The analytic model will then enable direct applications of the model to any system under any experimental conditions (temperature, strain rate, stress, dislocation density) in terms only of the underlying material parameter $\Delta\tilde{E}_p$, $w_* = w/2$, and L. Specifically, Magdon et al. [26] showed that the mean maximum minus minimum of the continuous Wiener process could be written as $-\frac{2\sigma^2}{\mu}Q_p\left(\frac{\mu^2 N}{2\sigma^2}\right)$ where $Q_p(x)$ is a tabulated function and σ and $\mu \le 0$ are the standard deviation and the drift bias of the process and N denotes the total number of uncorrelated steps. Applied to the kink migration problem, $\sigma = \Delta E_p\bar{w}^{1/2}$, $\mu = -ab^2\bar{w}\tau$, and $N = L/(b\bar{w})$. When these

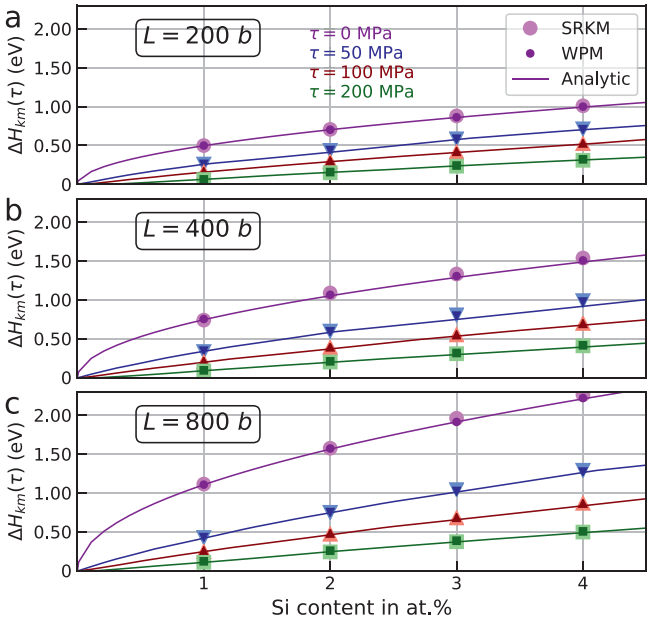

Fig. 7. Single-kink migration barrier $\Delta H_{\rm km}$ versus Si concentration as predicted by the SRKM, WPM, and analytic result, Eq. (10), at various applied stresses τ as indicated for migration distances L of (a) $200b$, (b) $400b$, and (c) $800b$ in the model Fe-Si alloys.

relationships are substituted into the result of Magdon et al., we obtain

$$\Delta H_{\rm km} = \frac{2\Delta\tilde{E}_p^2}{ab^2\tau}Q_p\left(\frac{a^2b^4\tau^2L/b}{2\,\Delta\tilde{E}_p^2}\right) = 2\Delta\tilde{E}_p\frac{\tau_c}{\tau}Q_p\left(\frac{\tau^2}{\tau_c^2}\frac{L}{2b}\right); \qquad \tau_c = \frac{\Delta\tilde{E}_p}{ab^2}, \quad (8)$$

where the characteristic stress τ_c is the stress required to overcome a single typical kink energy difference $\Delta\tilde{E}_p$ over unit glide distance b. Interestingly, the kink width $\bar{w}$ no longer appears in the barrier, and the barrier scales directly with the fundamental energy $\Delta\tilde{E}_p$. This result demonstrates why the WPM and SRKM are essentially identical at lengths $L/b >> 1$.

The kink migration is discrete, and the discrete-time Wiener process involves an additional correction term that is a function of σ and the discrete interval length (here $\bar{w}$) [27]. The Wiener process also does not nominally apply when the activation distance is $z^*/b < \bar{w}$. We can thus derive a correction factor by imposing the requirement that the energy barrier at the minimum WPM dis-

tance $L/b = \bar{w}$ is zero at the stress $\tau = \frac{\Delta\tilde{E}_p\sqrt{\bar{w}}}{qb^2\bar{w}}$ that is needed to overcome the average single-step barrier in the WPM. This leads to a correction factor $-2Q_p(\frac{1}{2})\Delta\tilde{E}_p\sqrt{\bar{w}}$. The coefficient $-2Q_p(\frac{1}{2}) = -0.926$, however, does not yield sufficiently agreement with the simulations and so we fit the numerical prefactor as -1.24 to best-match the WPM simulations, obtaining

$$\Delta H_{\rm km} = \Delta\tilde{E}_p\left[2\frac{\tau_c}{\tau}Q_p\left(\frac{\tau^2}{\tau_c^2}\frac{L}{2b}\right) - 1.24\bar{w}^{\frac{1}{2}}\right] \tag{9}$$

The function $Q_p(x)$ with $x \equiv \frac{\tau}{\tau_c}\sqrt{\frac{L}{2b}}$ remain tabulated only. However, we can accurately ($\sim 2\%$) approximate $Q_p(x^2)x^{-1} = 1.63(x+1.91)^{-1} + 0.025$ over the full range of x relevant in applications. Hence, a fully-analytic result for the kink migration barrier is then, after a bit of algebra, obtained as

$$\Delta H_{\rm km} = \Delta\tilde{E}_p\left[3.26\left(\frac{\tau}{\tau_c} + \frac{2.7}{\sqrt{L/b}}\right)^{-1} + 0.035\sqrt{L/b} - 1.07\sqrt{w/b}\right] \tag{10}$$

where we have also reverted to using the true kink width w. The results of the analytical solution, Eq. (10) for relatively short dislocation segments of $L/b = 200, 400,$ and 800 versus the Si concentration at various applied stresses are shown in Fig. 7. Excellent agreement is obtained with the previous stochastic simulations which demonstrates the accuracy of this fully analytical solution. Introducing the correction factor introduces a very small error in the activation volume $V_{\rm act} = z^*ab$, as discussed in Appendix B.

Before comparing the analytic model to more simulations with longer dislocation lengths, we discuss the final step of connecting the kink migration model to the double-kink nucleation/kink migration problem of physical interest. In the real physical problem, two kinks are nucleated and migrate away from each other. The implicit assumption in essentially all models of the overall plasticity process is that the next double-kink nucleation and kink migration event should only occur after the previous process is complete. Retaining this assumption, each of the two kinks experiences a similar statistical process but the migration distances $L_{\rm right}$ and $L_{\rm left}$ are different because the double-kink nucleation may occur anywhere along the total length $L = L_{\rm right} + L_{\rm left}$ with equal probability. Since the migration barrier increases with L, the kink with the longer migration path will typically encounter the largest barrier, and hence be the slowest process. The larger of the two sections is then randomly distributed in the range $(L/2, L)$ with an average of $3L/4$.

We thus adapt the SRKM to account for the double-kink nucleation process. For a dislocation of length L with stochastic energies assigned for each section of width b, we use the solute/double-kink interaction energy developed in [11] to find the most favorable nucleation site along the entire line. The left and right kinks are nucleated at this location and the kinks migrate through their remaining landscapes of lengths $L_{\rm right}$ and $L_{\rm left}$, respectively. The energy landscape for each kink is computed (Eq. 6) from which the stress-dependent kink migration barrier $\Delta E_{km}(\tau)$ is computed. We perform twenty thousand realizations for three dislocation lengths $L/b = 500, 1000, 2000$. For each realization, we determine the right and left migration distances $L_{\rm right}$ and $L_{\rm left}$ and the two associated migration barriers. The relevant barrier is the one corresponding to the longer of the lengths $L_{\rm right}$ and $L_{\rm left}$. Although there are cases where the largest barrier is found along the shorter path, their effects on the mean migration barrier are negligible (a few %). We thus apply the WPM at the mean $3L/4$ of the longest segment, leading to $N = L/w$. The results of the SRKM and WPM models are shown in Fig. 8, and excellent agreement is obtained. Finally, Fig. 8 also shows the analytical result for the mean migration barrier, Eq. (10). The agreement is again excellent, demonstrating the accuracy of the fully analytical solution in this regime.

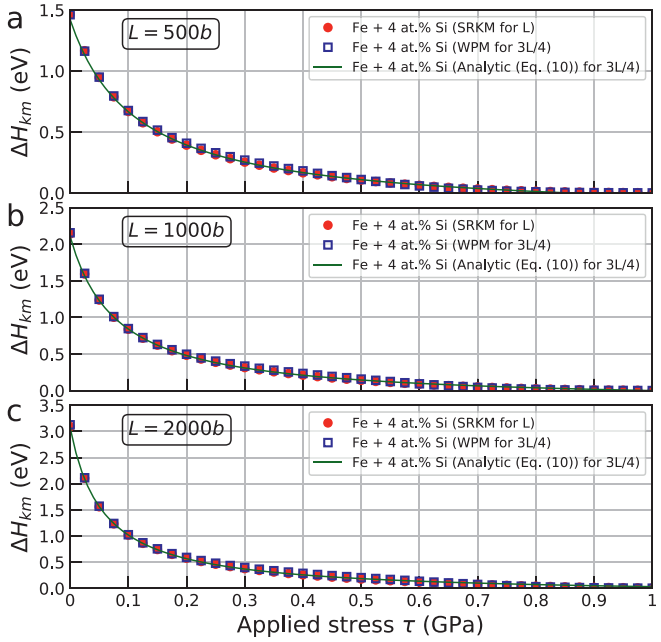

Fig. 8. Migration barrier $\Delta H_{\rm km}$ as computed by the SRKM, WPM, and fully-analytic theory versus applied stress τ for dislocations with length L (a) $500b$, (b) $1000b$, and (c) $2000b$ in Fe-4at.%Si model alloy.

5. Applications

The analytic theory of kink-migration has been extensively verified against simulations. This enables us to apply the theory with confidence to real BCC alloy systems in the dilute limit. Here we combine the kink migration theory with our recent double-kink nucleation theory to examine the transition from solute softening to solute strengthening in several dilute binary alloys. The challenges in comparing predictions to experimental data mostly lie in obtaining accurate input data, especially the solute/screw interaction energies, and accurate experimental results.

Experiments measure yield strength versus temperature and/or strain rate. Results here for the activation barrier are thus related to experiments via a standard thermally-activated Arrhenius model and Orowan's law. The total rate of dislocation motion in terms of the rates $r_{\rm dk}$ for double-kink nucleation and $r_{\rm km}$ for kink migration is

$$r = \left(\frac{1}{r_{\rm dk}} + \frac{1}{r_{\rm km}}\right)^{-1}. \tag{11}$$

Under almost all conditions, either $r_{\rm dk}$ or $r_{\rm km}$ dominates the rate and thus the total rate is expressed as

$$r = \nu_0 \exp\left(-\frac{\Delta H(\tau)}{kT}\right), \tag{12}$$

where the rate-controlling $\Delta H(\tau)$ is the larger of the double-kink nucleation and migration barriers and ν_0 is an appropriate attempt frequency [28]. As noted in the introduction, the temperature- and stress- plastic shear strain rate $\dot{\epsilon}$ at applied stress τ follows from Orowan's law as $\dot{\epsilon} \approx \rho bar$ and hence

$$\dot{\epsilon} = \dot{\epsilon}_0 \exp\left(-\frac{\Delta H(\tau)}{kT}\right), \tag{13}$$

where $\dot{\epsilon}_0 = \rho ba\nu_0$ is the reference strain rate. Experiments impose a temperature and strain rate, and hence an experimental enthalpy barrier $\Delta H^{\rm exp} = kT\,\log(\dot{\epsilon}_0/\dot{\epsilon})$.

Inverting Eq. (10) gives the yield stress required to achieve the imposed experimental enthalpy barrier as

$$\tau(\dot{\epsilon},T)=\tau_c\left[3.26\left(\frac{\Delta H^{\rm exp}}{\Delta\tilde{E}_p}-0.035\sqrt{L/b}+1.07\sqrt{w/b}\right)^{-1}-2.7\sqrt{b/L}\right] \quad (14)$$

Eq. (14) constitutes our analytical model for the migration-controlled strength as a function of temperature and strain rate. The only inputs to the theory are the solute/dislocation interaction energies that determine $\Delta\tilde{E}_p$, the dislocation line length, and kink width. The reference strain rate appears in a logarithm and thus has modest quantitative effects. Moreover, in real physical problems where the dislocation length is very large, $L\sim 2\times 10^3 b$, the kink width has rather small effects on final strength predictions.

Double-kink nucleation occurs at one of the most favorable local region of solute fluctuations for the process. At low temperatures when the most-favorable region dominates, the barrier can be written as

$$\Delta H_{\rm dk}(\tau)=\Delta H^0(\tau)+\Delta\bar{H}^{\rm sol}(c,N,\tau). \quad (15)$$

Here, $\Delta H^0(\tau)$ is the nucleation enthalpy barrier of the pure matrix which often takes the form of a Kocks law [29] $\Delta H^0(\tau)=\Delta H^0(0)[1-(\tau/\tau_p^0)^p]^q$ where p and q are fitting parameters and $\Delta H^0(0)$ and τ_p^0 are the zero-stress enthalpy barrier and pure Peierls stress, respectively. The solute contribution $\Delta\bar{H}^{\rm sol}(c,N,\tau)$ is the mean largest reduction in activation energy among all the $N=L/2w$ segments, and is [11]

$$\Delta\bar{H}^{\rm sol}=\Delta\tilde{E}_p G(\tau)\frac{\log(4\pi\log N)-4\log N-1.1544}{\sqrt{8\log N}}, \quad (16)$$

where $G(\tau)$ describes the stress-dependent double-kink transition state shape in the pure BCC metal under stress. At higher temperatures, additional regions could contribute to enhance the rate. We will use the full solution, as given in [11], in results shown below using the equations in [11]. Of importance here is that all of the effects of solutes on the nucleation barrier depend on exactly the same material parameters as derived here for the migration barrier ($\Delta\tilde{E}_p$, w, dislocation length L).

With theory for both the migration barrier $\Delta H_{\rm km}(\tau,L)$ and the nucleation barrier $\Delta H_{\rm dk}(\tau,L)$, the stress and temperature regimes of the controlling plasticity mechanism can be found. A schematic result of the two barriers versus stress, using parameters for real W-Re (see below), is shown in Figs. 9(a),(b), and (c) for W-1%Re, W-3%Re, and W-10%Re, respectively. With increasing solute concentration and at any specified stress, the barrier for nucleation is decreasing and the barrier for migration is increasing. Experimental conditions of temperature and strain rate determine the accessible barrier as $\Delta H^{\rm exp}$ and the highest-strength mechanism controls the strength under those conditions. The experimental barrier at T=300K and $\dot{\epsilon}=5.5\times10^{-4}$/s is shown in the Figs. 9. At 1%Re, yield is controlled by double-kink nucleation and is lower than pure W (solute softening). At 3% Re kink migration controls the strength but the double-kink nucleation strength is only slightly lower; the alloy is still softer than pure W. At 10% Re, the kink migration continues to control the strength, with the double kink nucleation stress now being much lower. This demonstrates the transition in mechanism. Furthermore, at 10% Re, the alloy is stronger than pure W, demonstrating solute strengthening. At a higher temperature, $\Delta H^{\rm exp}$ is higher and both the mechanism transition and onset of strengthening relative to pure W occur at a lower concentration. For example, but not shown, at T=650K ($\Delta H^{\rm exp}=936$ meV), the strength of W-3% Re is migration controlled and slightly larger than that of pure W.

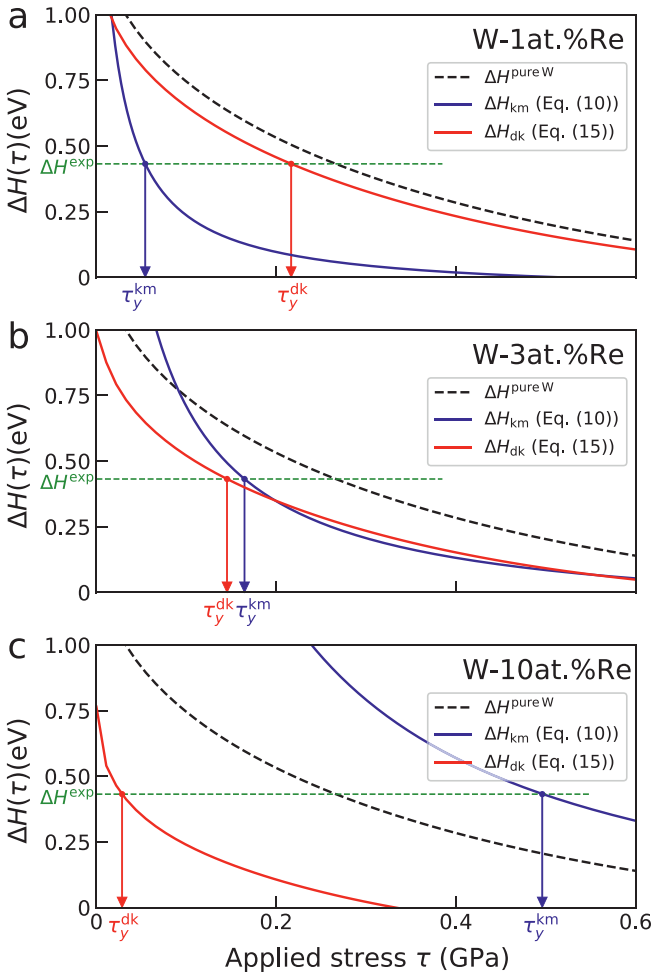

Fig. 9. Predicted barriers for double-kink nucleation $\Delta H_{\rm dk}$ (red) and kink-migration $\Delta H_{\rm km}$ (blue) versus applied stress τ, using parameters for W-Re at (a) W-1%Re, (b) W-3%Re, and (c) W-3%Re alloys. For illustration, an experimentally imposed $\Delta H^{\rm exp}=0.43$ eV corresponding to T=300K and $\dot{\epsilon}=5.5\times10^{-4}$/s is shown and the strength of each mechanism is indicated. The higher strength sets the alloy yield stress. A transition from double-kink nucleation to kink migration control of the strength is observed with increasing Re concentration. The barriers and strength for pure W are also shown, illustrating regimes of alloy softening and hardening relative to pure W.

5.1. Fe-Si alloys

Experimental yield stresses for Fe-Si (0.52 at%, 1.3 at%, 3.2 at%, and 5 at%) alloys versus temperature at a strain rate of $1.7\times10^{-4}{\rm s}^{-1}$ were reported by [30]. Other data by [31] at 1 and 4 at%, shown previously [22], is slightly lower than the data used here, and so the experimental results are not definitive. For predictions, we use a reference strain rate of $10^4{\rm s}^{-1}$, a dislocation density of $\rho=10^{12}m^2$ [32] and kink width $w=12b$ [11] obtained by GAP for pure Fe [33]. The solute/dislocation interaction energy parameter $\Delta\tilde{E}_p=178\sqrt{c}$ meV was obtained previously by Maresca et al. [15] as the value needed to fit data at 5at% using their non-dilute theory, with good agreement of that model at all higher concentrations. The interaction energy parameter differs from that of the model Fe-Si EAM potential because the EAM potential is not quantitative for real Fe-Si.

Fig. 10 shows the strength vs. temperature as measured and as predicted by various mechanisms. The data for pure Fe is shown for reference. The predictions are made for the kink migration model presented here, the double-kink nucleation model (Eqs. (9),(14),(20) [11]), and also the non-dilute model of Maresca et al. applied at these lower concentrations. The strength-controlling

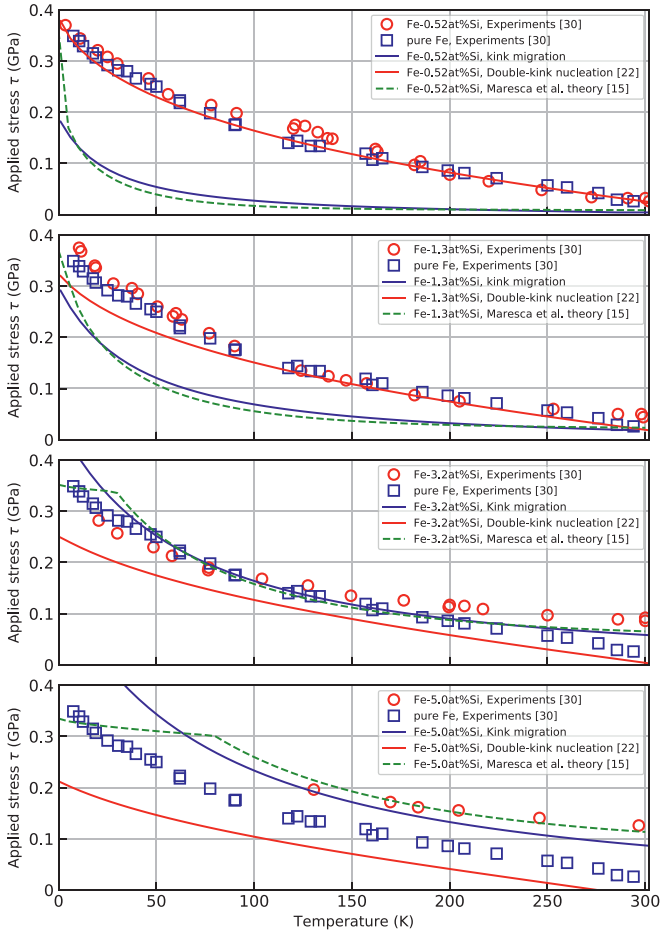

Fig. 10. Yield strength versus temperature, as predicted for the double-kink nucleation model, kink migration model, and non-dilute model, $Fe_{1-x}Si_x$ alloys at the concentrations shown.

mechanism is the mechanism with the highest strength at a given concentration and temperature. At the low concentrations of 0.52 at.%, double-kink nucleation is the controlling mechanism, with both kink migration strength and the non-dilute theory being much lower than experiments; the theory predicts almost no solute effects while experiments appear to show a slight strengthening (but see Ref. [22]). At 1.3 at.%, double-kink nucleation continues to control strength over nearly the entire temperature range. However, both kink migration and the non-dilute theory are close to the nucleation strength near T=300K. At 3.2 at.%, a transition in mechanism is predicted. The kink migration strength is higher than the double-kink nucleation strength over the entire temperature range. The experiments show a clear strengthening at higher T, consistent with predictions but slightly higher. At this concentration, in spite of different contributions to the total strengthening, the non-dilute strength is predicted to be nearly identical to the kink migration strength, with differences only at very low T. The nucleation-to-kink-migration and dilute-to-non-dilute transitions thus occur at essentially the same concentration. Then, at the higher concentration of 5.0 at.%, the alloy strength is significantly higher than that of pure Fe, the kink migration strength is also much higher but below the experiments, and the non-dilute theory captures the experiments with $\Delta\tilde{E}_p$ having been fit to this data.

As discussed previously, other literature data on Fe-Si shows very small softening at 1%Si and slightly less strengthening at 4at%, both being more consistent with theory. With such uncertainties in the experiments, we consider the parameter-free predictions here

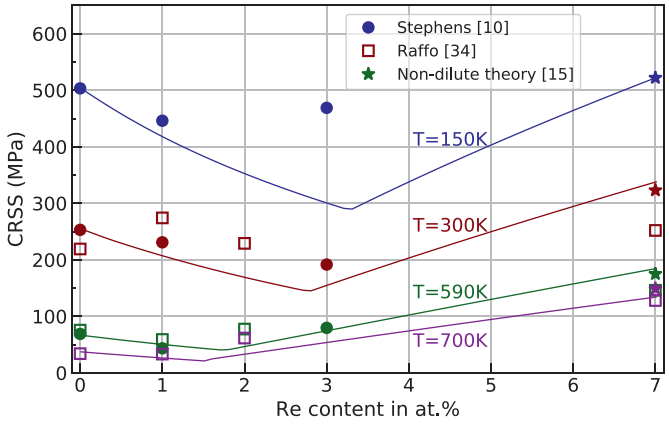

Fig. 11. Critical resolved shear stress (CRSS) versus solute concentration at various temperatures (blue: T=150K; red: T=300K; green: T=590K; purple: T=700K) for dilute W-Re alloys. Experiments (filled symbols: data from Stephens [10]; open symbols: data from Raffo [34]); present theory (solid lines); non-dilute theory at 7%Re [15] (bold ⋆ symbols)

to capture the major trends versus temperature and concentration quite well. We also conclude, however, that there is only a very narrow concentration around 3at% where the kink migration mechanism may control strength but where the non-dilute mechanisms give nearly identical results. Thus, while increasing Si in Fe-Si shows very weak (if any) softening followed by hardening, the traditional transition from nucleation to migration is quickly superseded by the non-dilute theory/mechanisms.

5.2. W-Re alloys

We now turn to the W-Re system and examine the yield stress of this alloy over a wide concentration range and temperatures T=150K, T=300K, T=590K, and T=700K. Experimental data are reported by [10] and [34] which were performed at nearly identical strain rates of $5.5\times10^{-4}s^{-1}$ and $8.3\times10^{-4}s^{-1}$. We again take $\rho=10^{12}m^{-2}$ ($L=1\mu m$), as a typical value for well-annealed metals, and $\dot{\epsilon}_0=10^4s^{-1}$. The kink width in pure W is taken as $12b$ [11]. The data on pure W reported by [10] is used to fit the Kocks model parameters $\Delta H_0=1.4$ eV, $\tau_p^0=1.1$ GPa,$p=0.49$, $q=1.69$. Note that this fit does not have high accuracy due to the limited data but that it only appears in the double-kink migration model and does not affect kink migration predictions. The solute/dislocation interaction energies were computed previously by first-principles DFT [35] from which the solute/dislocation interaction energy is obtained as $\Delta\tilde{E}_p=345\sqrt{c}$ meV. Strength is again predicted as the larger of the nucleation and migration strengths. There are no adjustable parameters.

Predictions of the strength versus Re concentration for several temperatures are shown in Fig. 11 along with the experimental data. The experiments are not definitive: the two datasets at T=300K show some differences at low concentrations. Nonetheless, the data generally show a transition from softening to hardening with increasing Re at temperatures up to 590K and no softening at 700K. The theory predicts the transition from softening to hardening at all temperatures, but with very little softening at 700K. The concentration at the transition is predicted to decrease with increasing temperature, as observed for 300K, 590K, and 700K. The experiments at 150K suggest a transition below 3%, with strengthening; this is a significant quantitative deviation between experiment and theory that remains unexplained. However, the experiments and theory at T=300K suggest a transition around 3%, and there is no mechanistic theory that would predict that the transition concentration increases with increasing temperature, so the experiments at T=150K and 3% Re are inconsistent with any model.

The 7at.%Re alloy is predicted to be in the strengthening regime at all the temperatures studied (300, 590, 700K) and there is very good quantitative agreement with available experiments.

Predictions of the non-dilute theory of Maresca et al. [15] at 7at.%Re are also shown in Fig. 11, and also agree very well with experiments and the kink migration strength. Thus, as for Fe-Si around 3%Si, there is also a concentation domain in W-Re (7% Re) where dilute and non-dilute theories give very similar results, indicating a smooth transition.

Overall, the predictions for W-Re are in good quantitative and qualitative agreement with the totality of available experiments. Note that no material parameters (beyond those for pure W) were fitted to achieve this level of agreement. The parameters were chosen based on independent considerations. Hence, we consider the predictions of the essentially parameter-free fully-derived statistical models for double-kink nucleation [11] and kink migration (this work) to be quite good.

6. Discussion

We have developed an analytical theory for the stress-dependent kink migration barrier in random dilute BCC alloys. We have shown that the kink migration process under stress is essentially the random walk-type "Wiener process with drift". The material parameters in the theory are only (i) the solute/screw dislocation interaction energies leading to a single relevant energy quantity $\Delta\tilde{E}_p$, (ii) the total dislocation length L, and (iii) emerging to a play a minor role, the kink-width w in the pure metal. The theory has been extensively validated on a model Fe-Si alloy via NEB calculations and direct stochastic simulations. Combined with a recent double-kink nucleation theory that involves the same material quantities, we have thus established a fully-analytic model for strengthening of screw dislocations over the full temperature range in the dilute regime concentration. A transition from double-kink nucleation and softening to kink-migration and strengthening is predicted with increasing temperature and/or concentration. We also find a smooth transition from the dilute theory to a recent non-dilute theory in application to both Fe-Si and W-Re alloys.

Our derived theory rationalizes some results from the Suzuki model. At high temperatures, corresponding to low stresses, the second and third terms in the bracket of Eq. (10) can be neglected. Also, in real alloys the dislocation segments length are typically large and so $\frac{\tau}{\tau_c} \gg 2.7\sqrt{\frac{b}{L}}$. Then, setting the barrier equal to the experimental $\Delta H = kT\log(\dot{\epsilon}_0/\dot{\epsilon})$, the strength versus temperature can be estimated as

$$\tau \simeq \alpha' \frac{\Delta\tilde{E}_p^2}{kT\,b^3}, \tag{17}$$

where α' is nearly constant. The yield strength thus decreases as $\approx 1/T$ and increases linearly with solute concentration since $\Delta\tilde{E}_p^2 \propto c$. This rationalizes Suzuki's high-T estimate [2]

$$\tau \simeq \alpha \frac{E^2 c}{kT\,b^3}, \tag{18}$$

The agreement in scalings with T and c arises because Suzuki's counting of the fluctuations in total solutes passed as the kink glides over long distances is captured correctly. However, E and α differ from $\Delta\tilde{E}_p$ and α', leading to both qualitative and quantitative differences.

Existing kMC methods have also made simplifying assumptions about the solute/screw interactions and the kink structure. For instance, [14] show schematics of a sharp kink (pure edge) so that kink glide corresponds to very few solutes entering the advancing screw segments. In a real kink, extending over $10-20b$, the change in energy due to solutes entering and leaving the kink is more gradual (spread over $\sim 1/2$ the kink width). Our SRKM and WPM analysis demonstrate that the effect of the kink width is fairly small, especially at higher temperatures. The kink width is, however, critical for double-kink nucleation. Thus, kMC approaches to tackling the overall problem of nucleation and migration should include details such as accurate interactions and accurate representation of the kinks and double-kink nucleation process.

The motion of screw dislocations in BCC High Entropy Alloys has emerged as an important and challenging issue for theory. One contribution to the strengthening is due to kink migration barriers. Recent work has shown that screw motion in complex alloys depends on a generalized form of $\Delta\tilde{E}_p$ [15,28,36] as

$$\Delta\tilde{E}_p = \left(\sum_{i,j}\sum_n c_n \Delta U_{ij}^n(a)^2\right)^{\frac{1}{2}}, \tag{19}$$

where all atom types n are considered solutes, c_n is the concentration of atom type n, and ΔU_{ij}^n is the change in interaction energy of a type-n solute at position (x_i, y_j) with the dislocation of the average alloy (see [15,37]) as the dislocation glides by a. The results here do not directly apply to screw controlled HEAs because HEAs adapt to the local energy landscape by forming kinks spontaneously along their length. The dislocation segments are in low-energy environments rather than random environments, and this must be accounted for in assessing kink glide. These aspects will be discussed in future work. We further note that the strengthening in HEAs may be controlled by edge dislocations rather than screw dislocations [36], making the kink migration process irrelevant.

The present theory applies within the standard approximation that solute interactions are weak enough for (i) screw motion to occur one Peierls valley at a time and (ii) the screw core structure is not altered by the solutes. The present analysis can be adapted to address the first assumption, but that is well beyond the scope of the present work. The second approximation has been found suitable for most substitutional solutes but not for interstitial solutes such as C, N, and O [38–40]. Interstitial interactions in the core can also be very large such that even the annihilation of two kinks converging at the site of the interstitial is not sufficient to overcome the interstitial interaction energy. Thus, multiple kinks are required. These issues are beyond the scope of the present work, but the concepts here can be generalized to address some aspects of interstitial strengthening.

In summary, our nucleation and migration models provide a complete, accurate, and nearly analytical statistical theory of strengthening in dilute substitutional BCC alloys. The set of material properties is small, and the same properties enter both double-kink nucleation and kink migration theories. While obtaining these properties remains challenging, we believe the theory here cements the long-sought quantitative understanding of strengthening in dilute BCC alloys.

Declaration of Competing Interest

The authors declare that they have no known competing financial interests or personal relationships that could have appeared to influence the work reported in this paper.

Acknowlgedgments

The authors gratefully acknowledge support of this work from the Swiss National Science Foundation through a grant for the project entitled 'Harnessing atomic-scale randomness: design and optimization of mechanical performance in High Entropy Alloys', Project"200021_18198/1". They also thank Dr. Francesco Maresca (U. Groningen) for providing the theory predictions of the Maresca et al. theory for Fe-Si and W-Re.

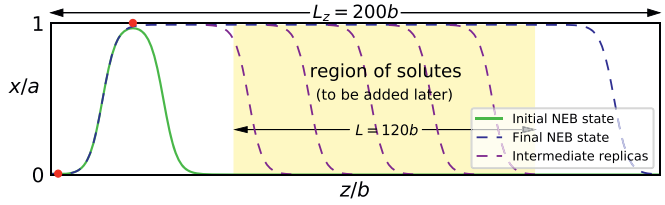

Fig. A.1. Atomistic modeling of single kink motion. The initial state for the NEB simulation is constructed by placing a single solute (top red dot) at the most favorable location and a second solute (bottom red dot) to inhibit motion of left sided kink. The final state of the kinked dislocation has the right kink at the far right of the sample. Executing NEB with no other solutes then generates a set of configurations (replicas) connecting the initial and final states and corresponding to kink glide. These replicas are then used as the initial path for subsequent NEB studies of the same kink motion through a field of solutes randomly distributed over the central length of $L = 120b$.

Appendix A. Simulation details of NEB calculations

To compute the minimum energy path (MEP) connecting the initial and final states, nudged elastic band (NEB) computations [41–44] are performed as implemented in LAMMPS [45]. The initial state of the NEB simulations was created as follows. Using the Fe lattice parameter, a rectangular simulation cell oriented with glide direction X $|||[1\bar{1}2]$, glide plane normal direction Y$|||[110]$, and dislocation line direction Z$|||[\bar{1}11]$ was constructed. Periodic boundary conditions are imposed along X and Z directions, while surfaces normal to the Y-direction are traction-free. The dimensions of the simulation cell are $L_x \sim 110$Å, $L_2 \sim 100$Å, and $L_z \sim 490$Å. A screw dislocation of Burgers vector $a/2[111]$ with line direction along Z is then introduced into the center of the cell by imposing a linear displacement $u_z = -bx/l_x$ for $0 < x < l_x$ on all atoms in the upper half of the simulation cell. Subsequently, two Si solutes in the proper locations, as discussed in 3.1, are added (see Fig. A.1). This generates the initial atomic configuration. The final state has the same structure as the initial state but shifted by a relative to the initial state. Atomic positions are then relaxed by using a combination of the FIRE algorithm [46] and relaxation of the cell dimensions. Convergence is achieved when the norm of the force vector fell below 10^{-6} eV/A and stresses σ_{XX}, σ_{XY}, and σ_{YY} fell below 0.1 MPa. An initial path of intermediate configurations (replicas) is constructed by linearly interpolating the atomic positions between the above relaxed initial and final states. We used 300 replicas and inter-replica spring constant was set to 10^{-2}eV/Å^2. Convergence was assumed when the maximum force acting on all of the atoms across all replicas was less than 1×10^{-3} eV/Å^2.

Appendix B. Activation volume

Here we address the activation volume V_{act}, of the thermally-activated kink-migration process. V_{act} is the Burgers vector multiplied by the area swept by the dislocation during the activation process and is computed as $V_{\text{act}} = -\partial \Delta H_{\text{km}}/\partial \tau$ [28]. At the $T = 0$K flow stress, which is the highest stress required for any kink migration, $V_{\text{act}} = 0$ is required. The activation volume from Eq. (10) is

$$V_{\text{act}} = ab^2 \left(0.55 \frac{\tau}{\tau_c} + \frac{1.5}{\sqrt{L/b}} \right)^{-2}. \tag{B.1}$$

This decays to zero only as $\tau \to \infty$. Due to the introduction of the correction factor, the energy barrier reaches zero at a finite τ with a finite V_{act}. This is also a flaw of the Suzuki model. However, in the present model, the activation volume at the $T = 0$K flow stress can be computed analytically as $V^* = ab^2 \left(0.019\sqrt{L/b} - 0.59\sqrt{w/b} \right)^2$ and at typical dislocation long lengths of $L \sim 2 \times 10^3 b$, $V^* \sim 0.1abw$, which is about one tenth of that obtained by Suzuki [2].

References

[1] E. Pink, R.J. Arsenault, Low-temperature softening in body-centered cubic alloys, Progress in Materials Science. 24 (1980) 1–50, doi:10.1016/0079-6425(79)90003-3.
[2] H. Suzuki, Solid solution hardening in body-centred cubic alloys, Dislocations in solids 4 (1980) 191–217.
[3] Caillard, Daniel, J.-L. Martin, Thermally activated mechanisms in crystal plasticity, Elsevier, 2003.
[4] A.S. Argon, Strengthening Mechanisms in Crystal Plasticity, Oxford University Press, Oxford, 2008.
[5] D.R. Trinkle, The chemistry of deformation: How solutes soften pure metals, Science 310 (2005) 1665–1667, doi:10.1126/science.1118616.
[6] Y.-J. Hu, M.R. Fellinger, B.G. Butler, Y. Wang, K.A. Darling, L.J. Kecskes, et al., Solute-induced solid-solution softening and hardening in bcc tungsten, Acta Materialia. 141 (2017) 304–316, doi:10.1016/j.actamat.2017.09.019.
[7] A. Sato, M. Meshii, Solid solution softening and solid solution hardening, Acta Metallurgica 21, no. 6 (1973) 753–768.
[8] B.V. Petukhov, Effects of point defects on dislocation mobility in crystals with high peierls barriers, Sov Phys Solid State 13 (1971) 1204–1207.
[9] J. Weertman, Dislocation model of low temperature creep, Journal of Applied Physics 29, no. 12 (1958) 1685–1689.
[10] J.R. Stephens, Dislocation structures in single-crystal tungsten and tungsten alloys, Metallurgical and Materials Transactions B. 1 (1970) 1293–1301, doi:10.1007/bf02900246.
[11] A. Ghafarollahi, F. Maresca, W. Curtin, Solute/screw dislocation interaction energy parameter for strengthening in bcc dilute to high entropy alloys, Modelling and Simulation in Materials Science and Engineering 27 (2019) 085011, doi:10.1088/1361-651x/ab4969.
[12] M.Z. Hossain, J. Marian, Stress-dependent solute energetics in WRe alloys from first-principles calculations, Acta materialia 80 (2014) 107–117.
[13] Y. Zhao, J. Marian, Direct prediction of the solute softening-to-hardening transition in WRe alloys using stochastic simulations of screw dislocation motion, Modelling and Simulation in Materials Science and Engineering 26 (4) (2018) 045002.
[14] S. Shinzato, M. Wakeda, S. Ogata, An atomistically informed kinetic monte carlo model for predicting solid solution strengthening of body-centered cubic alloys, International Journal of Plasticity 122 (2019) 319–337, doi:10.1016/j.ijplas.2019.03.004.
[15] F. Maresca, W.A. Curtin, Theory of screw dislocation strengthening in random BCC alloys from dilute to high-entropy alloys, Acta Materialia. 182 (2020) 144–162, doi:10.1016/j.actamat.2019.10.007.
[16] Cai, Wei, V.V. Bulatov, S. Yip, A.S. Argon, Kinetic monte carlo modeling of dislocation motion in BCC metals, Materials Science and Engineering: A 309 (2001) 270–273.
[17] Cai, Wei, V.V. Bulatov, J.F. Justo, A.S. Argon, S. Yip, Kinetic monte carlo approach to modeling dislocation mobility, Computational materials science 23 (1-4) (2002) 124–130.
[18] Mohri, Tetsuo, Y. Chen, M. Kohyama, S. Ogata, A. Saengdeejing, S.K. Bhattacharya, M. Wakeda, S. Shinzato, H. Kimizuka, Mechanical properties of fe-rich si alloy from hamiltonian, npj Computational Materials 3 (1) (2017) 1–14.
[19] Zhou, Xinran, S. He, J. Marian, Cross-kinks control screw dislocation strength in equiatomic bcc refractory alloys, Acta Materialia 211 (2021) 116875.
[20] Stukowski, Alexander, D. Cereceda, T.D. Swinburne, J. Marian, Thermally-activated non-schmid glide of screw dislocations in w using atomistically-informed kinetic monte carlo simulations, International Journal of Plasticity 65 (2015) 108–130.
[21] Ji, Rigelesaiyin, T. Phan, H. Chen, L. Xiong, Quantifying the dynamics of dislocation kinks in iron and tungsten through atomistic simulations, International Journal of Plasticity 128 (2020) 102675.
[22] Ghafarollahi, Alireza, William, A. Curtin, Theory of double-kink nucleation in dilute BCC alloys, Acta Materialia 196 (2020) 635–650.
[23] L. Proville, D. Rodney, M.C. Marinica, Quantum effect on thermally activated glide of dislocations, Nature Materials. 11 (2012) 845–849, doi:10.1038/nmat3401.
[24] L. Ventelon, F. Willaime, E. Clouet, D. Rodney, Ab initio investigation of the peierls potential of screw dislocations in bcc fe and w, Acta Materialia. 61 (2013) 3973–3985, doi:10.1016/j.actamat.2013.03.012.
[25] Durrett, Rick, Probability: theory and examples 49 (2019). Cambridge university press
[26] Magdon-Ismail, Malik, A.F. Atiya, A. Pratap, Y.S. Abu-Mostafa, On the maximum drawdown of a brownian motion, Journal of applied probability 41 (1) (2004) 147–161.
[27] L. Rogers, G. Christopher, S.E. Satchell, Estimating variance from high, low and closing prices, The Annals of Applied Probability (1991) 504–512.
[28] Varvenne, Cline, G.P.M. Leyson, M. Ghazisaeidi, W.A. Curtin, Solute strengthening in random alloys, Acta Materialia 124 (2017) 660–683.
[29] U.F. Kocks, A.A. S., A.M. F., Thermodynamics and kinetics of slip, 1975.
[30] K. Kitajima, Y. Aono, H. Abe, E. Kuramoto, Solid solution hardening and softening in iron alloy single crystals between 4.2 k and 300 k, Strength of Metals and Alloys (1979) 965–970, doi:10.1016/b978-1-4832-8412-5.50161-2.

[31] Y.T. Chen, D.G. Atteridge, W.W. Gerberich, Plastic flow of fe-binary alloys i. a description at low temperatures, Acta Metallurgica 29 (6) (1981) 1171–1185.
[32] S. Takeuchi, Solid-solution strengthening in single crystals of iron alloys, Journal of the Physical Society of Japan 27 (1969) 92–940, doi:10.1143/jpsj.27.929.
[33] F. Maresca, D. Dragoni, G. Csnyi, N. Marzari, W.A. Curtin, Screw dislocation structure and mobility in body centered cubic fe predicted by a gaussian approximation potential, Npj Computational Materials. 4 (2018), doi:10.1038/s41524-018-0125-4.
[34] Raffo, L. Peter, Yielding and fracture in tungsten and tungsten-rhenium alloys, Journal of the Less Common Metals 17 (2) (1969) 133–149.
[35] L. Romaner, Unpublished research.
[36] F. Maresca, W.A. Curtin, Mechanistic origin of high strength in refractory BCC high entropy alloys up to 1900k, Acta Materialia 182 (2020) 235–249, doi:10.1016/j.actamat.2019.10.015.
[37] Varvenne, Cline, A. Luque, W.G. Nhring, W.A. Curtin, Average-atom interatomic potential for random alloys, Physical Review B 93 (10) (2016) 104201.
[38] B. Lthi, L. Ventelon, D. Rodney, F. Willaime, Attractive interaction between interstitial solutes and screw dislocations in bcc iron from first principles, Computational Materials Science 148 (2018) 21–26.
[39] S.I. Rao, C. Woodward, B. Akdim, O.N. Senkov, A model for interstitial solid solution strengthening of body centered cubic metals, Materialia 9 (2020) 100611.
[40] Hachet, Guillaume, L. Ventelon, F. Willaime, E. Clouet, Screw dislocation-carbon interaction in BCC tungsten: an ab initio study, Acta Materialia 200 (2020) 481–489.
[41] Henkelman, Jonsson, J Chem Phys 113 (2000) 9978–9985.
[42] Henkelman, Uberuaga, Jonsson, J Chem Phys 113 (2000) 9901–9904.
[43] Nakano, Comp Phys Comm 178 (2008) 280–289.
[44] Maras, Trushin, Stukowski, Ala-Nissila, Jonsson, Comp Phys Comm 205 (2016) 13–21.
[45] S. Plimpton, Fast parallel algorithms for short-range molecular dynamics, 1993, 10.2172/10176421.
[46] E. Bitzek, P. Koskinen, F. Ghler, M. Moseler, P. Gumbsch, Structural relaxation made simple, Physical Review Letters. 97 (2006), doi:10.1103/physrevlett.97.170201.